JACS
JOURNAL OF THE AMERICAN CHEMICAL SOCIETY
Cite This: J. Am. Chem. Soc. 2018, 140, 4477−4480
Communication
pubs.acs.org/JACS

Localized Symmetry Breaking for Tuning Thermal Expansion in ScF_3 Nanoscale Frameworks

Lei Hu,[†,§] Feiyu Qin,[†] Andrea Sanson,[‡] Liang-Feng Huang,[§] Zhao Pan,[†] Qiang Li,[†] Qiang Sun,[∥] Lu Wang,[†] Fangmin Guo,[⊥] Umut Aydemir,[§,#] Yang Ren,[⊥] Chengjun Sun,[⊥] Jinxia Deng,[†] Giuliana Aquilanti,[¶] James M. Rondinelli,[§] Jun Chen,*[,†] and Xianran Xing[†]

[†]Department of Physical Chemistry, University of Science and Technology Beijing, Beijing 100083, China
[‡]Department of Physics and Astronomy, University of Padova, Padova I-35131, Italy
[§]Department of Materials Science and Engineering, Northwestern University, Evanston, Illinois 60208, United States
[∥]International Laboratory for Quantum Functional Materials of Henan, School of Physics and Engineering, Zhengzhou University, Zhengzhou 450001, China
[⊥]X-Ray Science Division, Argonne National Laboratory, Argonne, Illinois 60439, United States
[#]Department of Chemistry, Koc University, Sariyer, Istanbul 34450, Turkey
[¶]Elettra Sincrotrone Trieste, Basovizza, Trieste I-34149, Italy

Supporting Information

ABSTRACT: The local symmetry, beyond the averaged crystallographic structure, tends to bring unusual performances. Negative thermal expansion is a peculiar physical property of solids. Here, we report the delicate design of the localized symmetry breaking to achieve controllable thermal expansion in ScF_3 nanoscale frameworks. Intriguingly, an isotropic zero thermal expansion is concurrently engineered by localized symmetry breaking, with a remarkably low coefficient of thermal expansion of about $+4.0 \times 10^{-8}$/K up to 675 K. This mechanism is investigated by the joint analysis of atomic pair distribution function of synchrotron X-ray total scattering and extended X-ray absorption fine structure spectra. A localized rhombohedral distortion presumably plays a critical role in stiffening ScF_3 nanoscale frameworks and concomitantly suppressing transverse thermal vibrations of fluorine atoms. This physical scenario is also theoretically corroborated by the extinction of phonon modes with negative Grüneisen parameters in rhombohedral ScF_3. The present work opens an untraditional chemical modification route to achieve controllable thermal expansion by breaking local symmetries in materials.

Chemical modification on crystallographic symmetry plays a critical role in achieving attractive performances of functional materials. Recently, emerging local symmetries, distinct from the average long-range crystallographic structure, have brought unusual physical properties, such as local dipoles in cubic PbTe thermoelectric material,[1] a lower local symmetry associated with enhanced T_c in the Fe(Se,Te) superconductor,[2] and the local tetragonal distortion found in cubic $Mn_3Cu_{1-x}Ge_xN$ antiperovskite manganese nitrides.[3a]

Negative thermal expansion (NTE) is a peculiar physical property, which is not only fundamental but also practical issues for physics and materials science.[4−8] This unusual feature derives from diverse attributes, such as low-frequency phonon modes in ZrW_2O_8,[4] charge transfer in $BiNiO_3$,[7] microstructural effects in $Ca_2RuO_{3.74}$ ceramics,[8] spontaneous polarization in $Pb(Ti,V)O_3$,[9] and magnetic phase transitions in $La(Fe,Si,Co)_{11}$ and $Tb(Co,Fe)_2$.[10] Until now, the controllable thermal expansion has been elaborately devised by traditional chemical substitutions, such as $Zr_{1-x}Sn_xMo_2O_8$[11] and MNF_6 (M = 3*d* transition metals, N = Zr or Nb) solid solutions,[12] and by the insertion of guest molecules or atoms in cavities of framework structures, like $N(CH_3)_4CuZn(CN)_4$[13a] and $(Li,Sc,Fe)F_3$.[13b]

Here, we report unconventional localized symmetry breaking to tailor controllable thermal expansion in ScF_3 nanoscale frameworks. Intriguingly, an isotropic zero thermal expansion (ZTE) is concomitantly achieved, with remarkably small linear coefficient of thermal expansion (CTE), $\alpha_l = +4.0 \times 10^{-8}$/K from 325 K up to 675 K. A restricted rotation model and stiff lattice geometry are confirmed by local vibrational dynamics investigations. This work provides a fresh approach to devise special thermal expansion properties in conventional magnetic or electronic NTE materials.

ScF_3 nanocrystals with different crystalline sizes were prepared by a single source pyrolysis method (see the experimental section in the Supporting Information). ScF_3 nanocrystals with distinct average sizes are denoted as S2 (~13.2 nm), S3 (~8.1 nm), and S4 (~6.3 nm). For comparison, bulk ScF_3, named as S1, was also prepared by the solid-state reaction method as a reference (Figure S1). ScF_3 crystallizes in the $Pm\bar{3}m$ cubic lattice, composed of corner-sharing ScF_6 octahedra (Figure S2). Temperature dependence of high-energy synchrotron X-ray diffraction (SXRD) patterns (λ = 0.117 418 Å) was utilized to investigate the lattice thermal expansion. It is interesting to notice that ScF_3 crystals with continuously reduced crystalline sizes (from S1 to S4) reveal highly distinct thermal expansion behavior (Figure 1a). The

Received: January 23, 2018
Published: March 20, 2018

DOI: 10.1021/jacs.8b00885
J. Am. Chem. Soc. 2018, 140, 4477−4480

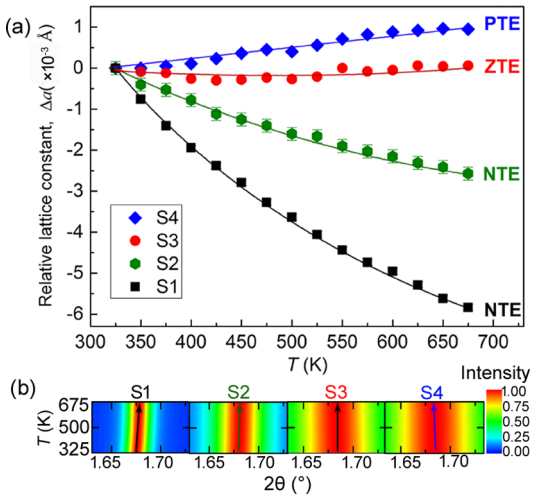

Figure 1. (a) Temperature dependence of relative lattice constant, $\Delta a = a_T - a_0$, of ScF_3 crystals. S1 is bulk ScF_3; whereas S2 (13.2 nm), S3 (8.1 nm), and S4 (6.3 nm) are nanocrystals. (b) Contour plots of (100) peaks of ScF_3 crystals (S1 to S4).

bulk ScF_3 (S1) shows a strong NTE with the linear CTE, $\alpha_l = -3.88 \times 10^{-6}$/K (325 to 675 K), consistent with the previous report.[14] However, the lattice thermal expansion of ScF_3 crystals can be well tuned by reducing crystalline sizes. The NTE is suppressed in sample S2 (13.2 nm), demonstrating a reduced $\alpha_l = -1.72 \times 10^{-6}$/K. Interestingly, an isotropic ZTE is achieved in sample S3 (8.1 nm). Its lattice constant nearly remains constant over a wide temperature range. Its CTE reaches a remarkably smaller value of $+4.0 \times 10^{-8}$/K (325 to 675 K). Further decreasing the crystalline sizes, the slightly positive thermal expansion (PTE) is achieved in sample S4 (6.3 nm), with $\alpha_l = +6.34 \times 10^{-7}$/K. Contour plots of (100) peaks of ScF_3 crystals (S1−S4) are presented in Figure 1b. The (100) peaks shift to different angle regions, directly affirming lattice NTE, ZTE, and PTE behaviors. Besides, the (100) peak width broadens with decreasing crystalline sizes, as clearly presented in Figure 1b.

In order to reveal the effect of local structure and lattice dynamics on tuning thermal expansion, we carried out complementary atomic pair distribution function (PDF) of synchrotron X-ray total scattering studies, Extended X-ray absorption fine structure (EXAFS) data, and first-principles calculations. Figure 2 shows the radial distribution functions, $R(r)$, of bulk (sample S1) and nano ScF_3 (sample S4) as a function of temperature. Two rotation models are suggested here, in which one is flexible rotation model and the other is restricted one (Figure 2a). The rotation dynamics can be directly revealed by the distance distribution of atomic pairs, such as the second and more distant Sc···F pairs corresponding to (1) and (2) in Figure 2a. As shown in Figure 2b, these peaks corresponding to atomic pairs are well observed, such as the peaks near 4.5 and 8.3 Å for the atomic pairs (1) and (2), marked by arrows in Figure 2a. In sharp contrast, there exist distinct distance distributions of atomic pairs with respect to temperature. In bulk S1, Sc···F pairs, (1) and (2), intensively drop in the amplitude and broaden in the width with rising temperature (marked by black boxes, Figure 2b), which supports the large atomic distance distribution and the flexible rotation model. In contrast, these peaks, (1) and (2), in nano ScF_3 (S4) seems to condense out at elevated temperatures, supporting the restricted rocking model. The relative bond

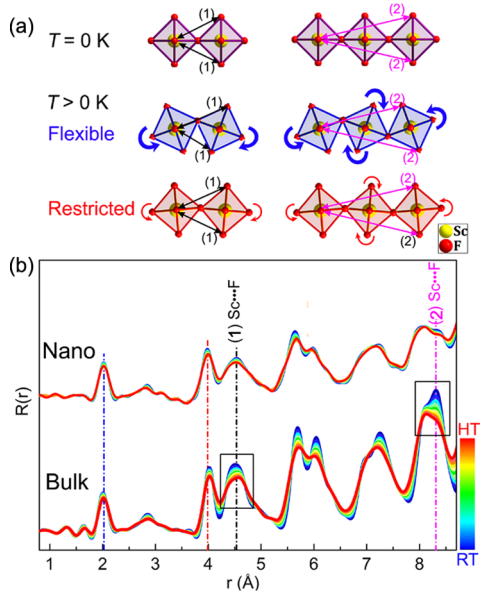

Figure 2. (a) Schematic view of vibrational models of ScF_6 octahedra. Two-end arrows indicate distinct atomic pairs. (b) Temperature dependence of $R(r)$s of bulk and nano ScF_3.

width, $\Delta\sigma^2(T)$, can be used to quantitatively describe the dynamics of atomic pairs (Figure S4). A larger slope of $\Delta\sigma^2$ versus T is observed in the NTE bulk ScF_3, which indicates soft atomic pairs and a flexible lattice geometry. However, the highly reduced slope is in the PTE nano ScF_3, in which rigid atomic pairs and restricted rotation model appears.

Derived from EXAFS data, the atomic mean square relative displacements (MSRDs), parallel ($MSRD_{\parallel}$) and perpendicular ($MSRD_{\perp}$) to the bond direction, can be utilized to understand the local vibrational dynamics of solids.[15] Figure 3 shows local vibrational dynamics of the Sc−F nearest-neighbors in bulk

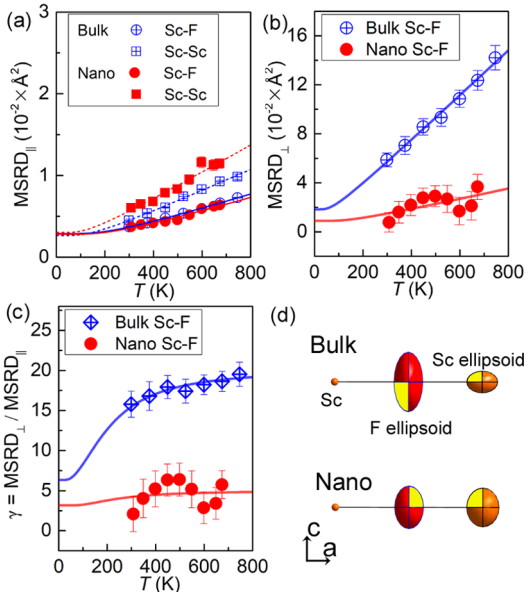

Figure 3. (a) Parallel $MSRD_{\parallel}$ of Sc−F and Sc−Sc. (b) Perpendicular $MSRD_{\perp}$ of Sc−F. (c) Anisotropy of relative thermal vibrations of Sc−F bonds ($\gamma = MSRD_{\perp}/MSRD_{\parallel}$). The lines are the best fits by utilizing the Einstein model. (d) Schematic illustration of relative thermal ellipsoids of Sc and F.

DOI: 10.1021/jacs.8b00885
J. Am. Chem. Soc. 2018, 140, 4477−4480

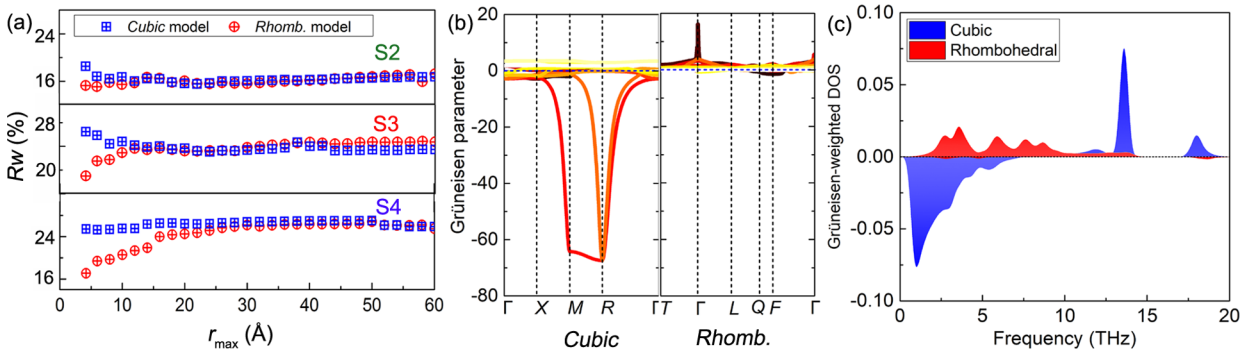

Figure 4. (a) Goodness of fits, R_w, as a function of r_{max} for S2, S3, and S4 with the cubic and rhombohedral models. (b) Grüneisen parameters for phonon modes in the Brillouin zone for the two bulk phases. (c) Grüneisen-weighted phonon density of states (DOS) in cubic and rhombohedral ScF_3, respectively.

(S1) and nano ScF_3 (S4). As shown in Figure 3a, they show a similar temperature response with effective bond-stretching force constants $\kappa_{\parallel}$, 9.38(7) and 9.94(9) eV/Å^2, respectively, estimated by the Einstein model fits. Also the $MSRD_{\parallel}$ of the second-neighbor Sc−Sc exhibits similar temperature dependence in bulk and nano ScF_3. In sharp contrast, a large discrepancy occurs in the perpendicular $MSRD_{\perp}$ (Figure 3b). For bulk ScF_3 (S1), the $MSRD_{\perp}$ of nearest-neighbors Sc−F strongly increases with increasing temperature, showing a small effective bond-bending force of relative thermal vibrations, monitored by the ratio $\gamma = MSRD_{\perp}/MSRD_{\parallel}$, as presented in Figure 3c. In bulk ScF_3, the value of γ increases up to as large as 20 at high temperatures, indicating a large transverse thermal vibration of fluorine. Such large γ has also been observed in other strong NTE compounds, like Ag_2O,[16a] $CuScO_2$[16b] or ZrW_2O_8.[17] In contrast, γ in the nanocrystal ScF_3 remains at much lower values, which reflects the highly reduced transverse thermal vibration. Additionally, Sc atoms exhibit isotropic dynamic character, determined by the MSRDs of the Sc−Sc second-neighbors (Supporting Information, Section 5). Figure 3d presents the sketch of relative thermal ellipsoids of F and Sc atoms in bulk and nano ScF_3. The strong NTE in bulk ScF_3 is associated with the strong transverse vibrations of the fluorine atoms through the "guitar-string" effect;[18] however, they are considerably suppressed in nano ScF_3.

To better understand the local structure symmetry, PDF refinements of different r ranges were implemented with both cubic ($Pm\bar{3}m$) and rhombohedral ($R\bar{3}c$) models from r_{min} of 1.4 Å to larger r_{max} (Figure 4a). It is interesting to find that the refinements of the rhombohedral symmetry are better than those of the cubic phase below a certain short r range. This indicates that the symmetry breaking only occurs locally but not globally. Furthermore, with increasing crystalline size, the symmetry breaking occurs in a smaller r range. Consequently, for a larger ScF_3 nanocrystal, the local symmetry change is not observed.[19] What is the driving force to induce the local rhombohedral distortion? Bulk ScF_3 transforms from a cubic phase into rhombohedral one under 0.5 to 0.8 GPa hydrostatic pressures.[14] The surface pressures increase rapidly with decreasing crystalline sizes from S2, S3 to S4, whose chemical surface pressures are comparable to the extrinsic hydrostatic pressures (see Figure S10). This behavior implies the localized rhombohedral distortion is generated by the surface pressure (the inset of Figure S10).

In order to elucidate the critical role of localized symmetry breaking in the phonon modes, *ab initio* theoretical calculations on phonon-related spectra and a ScF_3 nanocluster simulation were performed. Phonon modes with greater negative Grüneisen parameters emerge along the Brillouin zone, M and R directions, which contribute to NTE in bulk ScF_3, but they are eliminated in the rhombohedral phase (Figure 4b). Significantly, the phonon modes with negative Grüneisen parameters, dominate the low frequency region in the cubic symmetry (Figure 4c). In sharp contrast, phonon modes with positive Grüneisen parameters overwhelm most frequency regions in the rhombohedral phase. Besides, a strong distortion is found in the simulated ScF_3 nanocrystals (Figure S14b), which also supports the evidence of local symmetry breaking found in the PDF investigation.

The localized symmetry breaking drives fluorine atoms away from the straight linkage of Sc−F−Sc (inset of Figure S14a), which thereafter impedes thermal vibration of fluorine. It is in good agreement with the restricted rotational model (Figure 2a) and the smaller perpendicular $MSRD_{\perp}$ in ScF_3 nanocrystals (Figure 3b). With further decreasing crystalline sizes, the region of local symmetry breaking gradually grows and plays a significant role in the suppression of NTE. Consequently, the NTE of bulk ScF_3 is weakened to ZTE in sample S3 and ultimately transforms into PTE in sample S4.

It is known that tuning thermal expansion is a critical issue for the development of NTE solids. In this work, the localized symmetry breaking is proven to be an effective route to achieve controllable thermal expansion. Surprisingly, an isotropic ZTE is achieved in sample S3 over a wide temperature range (α_l = +4.0 × 10^{-8}/K, 325 to 675 K), which is comparable to the rare isotropic ZTE compounds (summarized in Table S2) achieved by conventional chemical modification methods, such as $Zr_{1-x}Sn_xMo_2O_8$ (α_l = −6.0 × 10^{-8}/K, 12−600 K),[11] $Mn_3(Ga_{0.5}Ge_{0.4}Mn_{0.1})N_{0.9}C_{0.1}$ ($|\alpha_l|$<5 × 10^{-7}/K, 190−272 K),[3b] $Mn_3Cu_{0.5}Ge_{0.5}N$ (1.2 × 10^{-7}/K, 12−230 K),[3c] $(Sc_{0.85}Ga_{0.05}Fe_{0.1})F_3$ (α_l = +2.3 × 10^{-7}/K, RT ∼ 900 K),[20] and $Zn_4B_6O_{13}$ (α_l = +2.8 × 10^{-7}/K, 13−110 K).[21]

In summary, the localized symmetry breaking is utilized to tune thermal expansion of ScF_3 crystals from negative to positive. Intriguingly, an isotropic ZTE is achieved over a wide temperature range. Both temperature dependence of the PDF and EXAFS gives fundamental insights into the local vibrational dynamics. The local structure analysis highlights a short-range symmetry breakdown from cubic to rhombohedral in ScF_3 nanocrystals. The localized symmetry breaking makes the lattice stiff, restricts the fluorine vibration, and thus suppresses the NTE. The present study provides a novel way to devise and

DOI: 10.1021/jacs.8b00885
J. Am. Chem. Soc. 2018, 140, 4477−4480

control thermal expansion of materials from the perspective of local structures.

■ ASSOCIATED CONTENT

Supporting Information

The Supporting Information is available free of charge on the ACS Publications website at DOI: 10.1021/jacs.8b00885.

Experimental and calculation details (PDF)

■ AUTHOR INFORMATION

Corresponding Author

*junchen@ustb.edu.cn

ORCID

Andrea Sanson: 0000-0003-3218-3553
Liang-Feng Huang: 0000-0003-2937-5183
James M. Rondinelli: 0000-0003-0508-2175
Jun Chen: 0000-0002-7330-8976
Xianran Xing: 0000-0003-0704-8886

Notes

The authors declare no competing financial interest.

■ ACKNOWLEDGMENTS

This work was supported by the National Natural Science Foundation of China (grant nos. 91422301, 21231001, and 21590793), the Changjiang Young Scholars Award, the National Program for Support of Top-notch Young Professionals, the Fundamental Research Funds for the Central Universities, China, and the Special Foundation of the Director of Technical Institute of Physics and Chemistry. L.F.H. and J.M.R. were supported by the Office of Naval Research under Grant No. N00014-16-1-2280 and the National Science Foundation under Grant No. DMR-1454688. The use of the Advanced Photon Source at Argonne National Laboratory was supported by the U.S. Department of Energy, Office of Science, Office of Basic Energy Sciences (DE-AC02-06CH11357). We acknowledge the ELETTRA Synchrotron Radiation Facility for provision of synchrotron radiation as well as all the staff of the XAFS beamline. We also thanks for the discussion with Prof. G. Jeffrey Snyder.

■ REFERENCES

(1) Božin, E. S.; Malliakas, C. D.; Souvatzis, P.; Proffen, T.; Spaldin, N. A.; Kanatzidis, M. G.; Billinge, S. J. L. *Science* **2010**, *330*, 1660.

(2) Louca, D.; Horigane, K.; Llobet, A.; Arita, R.; Ji, S.; Katayama, N.; Konbu, S.; Nakamura, K.; Koo, T.-Y.; Tong, P.; Yamada, K. *Phys. Rev. B: Condens. Matter Mater. Phys.* **2010**, *81*, 134524.

(3) (a) Iikubo, S.; Kodama, K.; Takenaka, K.; Takagi, H.; Takigawa, M.; Shamoto, S. *Phys. Rev. Lett.* **2008**, *101*, 205901. (b) Takenaka, K.; Takagi, H. *Appl. Phys. Lett.* **2009**, *94*, 131904. (c) Song, X.; Sun, Z.; Huang, Q.; Rettenmayr, M.; Liu, X.; Seyring, M.; Li, G.; Rao, G.; Yin, F. *Adv. Mater.* **2011**, *23*, 4690−4694.

(4) Mary, T. A.; Evans, J. S. O.; Vogt, T.; Sleight, A. W. *Science* **1996**, *272*, 90.

(5) Mohn, P. *Nature* **1999**, *400*, 18.

(6) (a) Attfield, J. P. *Nature* **2011**, *480*, 465. (b) Evans, J. S. *J. Chem. Soc., Dalton Trans.* **1999**, *19*, 3317.

(7) Azuma, M.; Chen, W. T.; Seki, H.; Czapski, M.; Oka, K.; Mizumaki, M.; Attfield, J. P. *Nat. Commun.* **2011**, *2*, 347.

(8) Takenaka, K.; Okamoto, Y.; Shinoda, T.; Katayama, N.; Sakai, Y. *Nat. Commun.* **2017**, *8*, 14102.

(9) Pan, Z.; Chen, J.; Jiang, X.; Hu, L.; Yu, R. Z.; Yamamoto, H.; Ogata, T.; Hattori, Y.; Guo, F.; Fan, X.; Li, Y.; Li, G.; Gu, H.; Ren, Y.; Lin, Z.; Azuma, M.; Xing, X. *J. Am. Chem. Soc.* **2017**, *139*, 14865.

(10) (a) Huang, R. J.; Liu, Y.; Fan, W.; Tan, J.; Xiao, F.; Qian, L.; Li, L. F. *J. Am. Chem. Soc.* **2013**, *135*, 11469. (b) Song, Y.; Chen, J.; Liu, X.; Wang, C.; Zhang, J.; Liu, H.; Zhu, H.; Hu, L.; Lin, K.; Zhang, S.; Xing, X. *J. Am. Chem. Soc.* **2018**, *140*, 602.

(11) Tallentire, S. E.; Child, F.; Fall, I.; Vellazarb, L.; Evans, I. R.; Tucker, M. G.; Keen, D. A.; Wilson, C.; Evans, J. S. *J. Am. Chem. Soc.* **2013**, *135*, 12849.

(12) Hu, L.; Chen, J.; Xu, J.; Wang, N.; Han, F.; Ren, Y.; Pan, Z.; Rong, Y.; Huang, R.; Deng, J.; Li, L.; Xing, X. *J. Am. Chem. Soc.* **2016**, *138*, 14530.

(13) (a) Phillips, A. E.; Halder, G. J.; Chapman, K. W.; Goodwin, A. L.; Kepert, C. J. *J. Am. Chem. Soc.* **2010**, *132*, 10. (b) Chen, J.; Gao, Q.; Sanson, A.; Jiang, X. X.; Huang, Q. Z.; Carnera, A.; Rodriguez, C. G.; Olivi, L.; Wang, L.; Hu, L.; Lin, K.; Ren, Y.; Lin, Z. S.; Wang, C.; Gu, L.; Deng, J. X.; Attfield, J. P.; Xing, X. R. *Nat. Commun.* **2017**, *8*, 14441.

(14) Greve, B. K.; Martin, K. L.; Lee, P. L.; Chupas, P. J.; Chapman, K. W.; Wilkinson, A. P. *J. Am. Chem. Soc.* **2010**, *132*, 15496.

(15) Fornasini, P.; Dalba, G.; Grisenti, R.; Purans, J.; Vaccari, M.; Rocca, F.; Sanson, A. *Nucl. Instrum. Methods Phys. Res., Sect. B* **2006**, *246*, 180.

(16) (a) Sanson, A.; Rocca, F.; Dalba, G.; Fornasini, P.; Grisenti, R.; Dapiaggi, M.; Artioli, G. *Phys. Rev. B: Condens. Matter Mater. Phys.* **2006**, *73*, 214305. (b) Ahmed, S. I.; Dalba, G.; Fornasini, P.; Vaccari, M.; Rocca, F.; Sanson, A.; Li, J.; Sleight, A. W. *Phys. Rev. B: Condens. Matter Mater. Phys.* **2009**, *79*, 104302.

(17) Sanson, A. *Chem. Mater.* **2014**, *26*, 3716.

(18) Hu, L.; Chen, J.; Sanson, A.; Wu, H.; Rodriguez, C.; Olivi, L.; Ren, Y.; Fan, L.; Deng, J. X.; Xing, X. R. *J. Am. Chem. Soc.* **2016**, *138*, 8320.

(19) Yang, C.; Tong, P.; Lin, J. C.; Guo, X. G.; Zhang, K.; Wang, M.; Wu, Y.; Lin, S.; Huang, P. C.; Xu, W.; Song, W. H.; Sun, Y. P. *Appl. Phys. Lett.* **2016**, *109*, 023110.

(20) (a) Hu, L.; Chen, J.; Fan, L.; Ren, Y.; Rong, Y.; Pan, Z.; Deng, J.; Yu, R.; Xing, X. J. *J. Am. Chem. Soc.* **2014**, *136*, 13566. (b) Hu, L.; Chen, J.; Fan, L. L.; Ren, Y.; Huang, Q. Z.; Sanson, A.; Jiang, Z.; Zhou, M.; Rong, Y. C.; Wang, Y.; Deng, J. X.; Xing, X. *Adv. Mater.* **2015**, *27*, 4592.

(21) Jiang, X. X.; Molokeev, M. S.; Gong, P. F.; Yang, Y.; Wang, W.; Wang, S. H.; Wu, S. F.; Wang, Y. X.; Huang, R. J.; Li, L. F.; Wu, Y. C.; Xing, X. R.; Lin, Z. S. *Adv. Mater.* **2016**, *28*, 7936.

DOI: 10.1021/jacs.8b00885
J. Am. Chem. Soc. 2018, 140, 4477−4480